

# Viscoelastic surface instabilities

A. Lindner<sup>a</sup> and C. Wagner<sup>b</sup>

<sup>a</sup> *Laboratoire de Physique et Mécanique des Milieux Hétérogènes (PMMH), UMR 7636 CNRS - ESPCI - Universités Paris 6 et 7, 10, rue Vauquelin, 75231 Paris Cedex 05, France*

<sup>b</sup> *Technische Physik, Universität des Saarlandes, Postfach 151150, 66041 Saarbrücken, Germany*

---

## Abstract

We review three different types of viscoelastic surface instabilities: The Rayleigh – Plateau, the Saffman – Taylor and the Faraday instability. These instabilities are classical examples of hydrodynamic surface instabilities. The addition of a small amount of polymers to pure water can alter its flow behavior drastically and the type of instability may change not only quantitatively but also qualitatively. We will show that some of the observed new phenomena can be explained by the use of simple rheological models that contain most of the underlying physical mechanisms leading to the instability. A quantitative description however is often only possible close to the onset of the instability or for weak deviations from Newtonian behavior. A complete theoretical description is still lacking when the system is driven far from equilibrium or for fluids with strong non-Newtonian behavior.

## Résumé

Nous discutons dans ce papier trois types d'instabilités interfaciales dans des liquides visco-élastiques : l'instabilité de Rayleigh – Plateau, l'instabilité de Saffman – Taylor et l'instabilité de Faraday. Ce sont toutes les trois des exemples typiques d'instabilités hydrodynamiques de surface. L'addition d'une faible quantité de polymères à de l'eau pure suffit à lui conférer un comportement fortement non-newtonien. Les instabilités dans ces solutions sont modifiées pas seulement de façon quantitative mais aussi dans leur nature. Nous montrons que des modèles rhéologiques simples peuvent expliquer l'origine des modifications observées sur les instabilités. Une description quantitative n'est en général possible uniquement près du seuil d'instabilité et uniquement pour des déviations faibles d'un comportement newtonien. Une description complète loin de l'équilibre et pour des propriétés non-newtoniennes fortes manque à ce jour.

---

## 1. Introduction

In this paper, we review three typical hydrodynamic surface (or more general interfacial) instabilities: the Rayleigh – Plateau instability, the Saffman – Taylor instability and the Faraday instability. These instabilities were chosen as they are each representative of a more general class of pattern-forming systems and we have investigated each. Here we discuss the modifications of these instabilities that occur when using viscoelastic fluids instead of simple Newtonian liquids.

One of the most prominent examples of a surface instability is a water droplet that detaches from a faucet (for a review see [1, 2]). The primary stages of the detachment of the droplet can be described by the linear Rayleigh – Plateau instability: a cylindrical thread is destabilized by surface tension and splits up into individual droplets, thus minimizing the energy of the system. In the non-linear regime, the final detachment or pinch-off of the droplet represents a so-called finite time singularity and must be described in a very different way, e.g., by use of so-called self similarity solutions. The generation of droplets also occurs in many industrial applications where, instead of simple liquids like water or oils, more complex liquids such as polymer melts, polymer solutions, surfactants, suspensions, etc. are processed. The hydrodynamics of these liquids differ from those of Newtonian liquids; as a result, the character of their surface instabilities can be altered dramatically. When a tiny amount of a flexible polymer is added to a solvent, pinch-off is strongly delayed and, in the nonlinear regime, a viscoelastic filament is formed between the nozzle and the droplet [3, 4, 5, 6, 7, 8, 9, 10, 11, 12]. Interestingly, this contrasts with theoretical predictions obtained from a linear analysis, in which an increase in growth rates and an acceleration of the break-off was predicted [3].

Experiments using yield stress fluids [13, 14] or granular suspensions [15] also reveal a strong alteration of the detachment process.

A classical pattern-forming system containing a free surface is the Faraday experiment [16]. When a layer of liquid is shaken vertically by a sinusoidal force, the flat interface becomes unstable as soon as a critical amplitude is exceeded. Standing waves of high symmetry are formed and patterns of lines, squares, hexagons, quasiperiodic patterns, superlattices and oscillons have been reported [17, 18, 19, 20, 21]. Energy is continuously fed into the system by the driving force and is dissipated by the viscous flow. This leads to a nonequilibrium situation in which the pattern selection process is no longer described by thermodynamic laws but only by the nonlinear dynamics of the system. For higher driving strengths, the pattern dynamics may become chaotic or weakly turbulent until droplet ejection occurs. Again, the introduction of a complex liquid can fundamentally alter the pattern selection process of the system [22, 23, 24, 25, 26, 27, 28].

Another classical example involving, in this case, a moving interface is the so-called Saffman–Taylor instability [29]. When a viscous fluid pushes a less viscous fluid in a narrow channel or Hele – Shaw cell, the interface between the two fluids becomes unstable and the formation of air fingers occurs. This instability has received much attention as an archetype of pattern-forming systems; it belongs to the class of free-boundary problems, in which the growth of the structures takes place in a Laplacian field [30]. A linear stability analysis yields a length scale that in combination with the geometry of the system also determines the non-linear growth of the viscous fingers observed. The Saffman – Taylor instability has been intensively studied for Newtonian fluids [31, 32, 33] and lately also for non-Newtonian fluids [34, 35] such as polymer or surfactant solutions [36, 37, 38, 39] foams, pastes, clays and gels [40, 41, 42, 35] and granular suspensions or dry granular media [43, 44, 45, 46]. The Saffman– Taylor instability is important for a number of applications, including oil recovery, coatings, and adhesive debonding [47]. These applications often involve non-Newtonian fluids, e.g., polymer solutions, which have been shown to fundamentally alter the selection process of the viscous fingers (see figure 8).

Further examples of hydrodynamic surface instabilities include the Kelvin – Helmholtz instability (the interfacial instability of two liquids that are sheared against each other), the Rayleigh–Taylor instability (that of the interface between two liquids of different densities with the heavier liquid placed on top of the lighter) , the Bénard Marangoni (an instability that occurs when a layer of liquid that is heated from below becomes unstable due to differences in the surface stresses caused by thermal gradients), the case in which a thin film flowing down an inclined plane becomes unstable against wavy distortion [48] and the disintegration of a liquid jet into droplets [2]. Some of these systems have been investigated for the case of complex liquids. A special case is the so-called shark-skin instability [49, 50], which refers to the appearance of a wavy distortion on a polymeric fiber that is forced through a hole or slit (a "die") above a critical speed. This instability is attributed either to an instability at the solid-liquid interface (stick-slip) or to a bulk instability [51].

For analytical and numerical investigations, treatment of the free interface of these systems is still a challenge. Despite the fact that these instabilities have been known for a long time, theoretical understanding of the underlying mechanisms was only obtained much later. The Faraday Experiment was the first hydrodynamic pattern-forming system that has been described scientifically [16]; however, a successful numerical analysis based on the full Navier – Stokes equation was performed only recently [52]. The pinch-off of a water droplet represents a very general problem; however, it was solved analytically only in the 1990s [53]. The Saffman – Taylor instability was described by Saffman and Taylor in 1958 [29], but the mechanism of finger selection in this instability has remained a puzzle for several decades. The problem was solved numerically in the '80s [54] but was only much later solved analytically [55, 56, 57]. Analytical treatment of the case of viscoelastic liquids remains challenging even today.

In this paper, we discuss experimental modification of the Rayleigh – Plateau (followed by the pinch-off of the droplet), the Saffman – Taylor and the Faraday instabilities when using one type of non-Newtonian fluids: polymer solutions. The addition of small amounts of either flexible or rigid polymers to pure water or water- glycerol mixtures can dramatically change the properties of the liquid. We show that the non-Newtonian properties of these solutions affect the three surface instabilities in very different ways, and further show that some of the observed new phenomena can be explained by the use of simple rheological models describing the hydrodynamics of the complex liquids. However, a quantitative description is often only possible close to the onset of the instability or for weak deviations from Newtonian behavior. A complete theoretical description is still lacking when the system is driven far from equilibrium or for strong non-Newtonian behavior.

## 2. The hydrodynamics of complex liquids

In this chapter, we discuss the hydrodynamics of polymer solutions and characterize the specific solutions that were used in the following studies. From a theoretical point of view, polymers represent very complex systems due to the large number of degrees of freedom that exist in their structures. Even a single polymer chain can possess millions of degrees of freedom due to the many independent molecular bonds between monomers that can rotate more or less freely. In equilibrium, entropic forces keep the polymer in a mainly coiled state that allows the highest number of conformations. A first approach to representing polymer structure is to model the polymer as a series of connected beads. If hydrodynamic interaction between the beads is taken into account, one obtains the so-called Zimm model [58]. This model predicts that a polymer that is deformed relaxes to its coiled equilibrium configuration with a certain relaxation time  $\tau_p$ . The relaxation time depends strongly on the molecular weight, the flexibility of the polymer and the viscosity of the solvent. It is worth pointing out that the polymer is an entropic spring only, and that in typical experiments, energies sufficient to affect the bonds are not reached. In dilute solution, polymers do not interact with each other. Higher concentrations can be referred to as semidilute as long as effects such as reptation modes, which are observed in polymer melts, are not present. The hydrodynamics of polymer solutions is challenging because it is not clear a priori how the coarse graining from the microscopic polymer models to a continuum mechanical description can be properly performed. Often, macroscopic models built on a heuristic base that can give some insight into the specific flow situation are used. A quantity that is often used to measure the importance of elastic effects under flow is the so-called Weissenberg number  $Wi = \tau_p \dot{\gamma}$ , with  $\tau_p$  the relaxation time of the solution and  $\dot{\gamma}$  the shear rate of the flow. It compares in that way the relaxation time of the polymer to the typical time scale of the flow. Only if the Weissenberg number is of  $O(1)$  the flow is strong enough to affect the polymers significantly.

In our experiments, we deal on the one hand with dilute solutions of the polymers xanthane and PEO (polyethylenoxide) and, on the other hand, with more concentrated solutions of PAA (polyacrylic-co-acrylacid). These polymers are important for a wide variety of applications. Xanthane is used to control the rheological properties of products such as tooth paste, yoghurt, curd and cream; PEO is used to reduce drag in turbulent flows and PAA is used as a shear thickener in paper coating applications. These solutions show some of the most frequently encountered non-Newtonian properties, making them excellent model systems. We now represent the rheology of these solutions and discuss their non-Newtonian behavior in detail.

Dilute or semi-dilute solutions of the rigid polymer xanthane ( $M_w = 3 * 10^6$  g/mol) are shear-thinning. Figure 1 shows the shear viscosity obtained for solutions of various concentrations of xanthane. With increasing concentration, an increased viscosity at low shear rates and increasingly strong shear thinning when  $\dot{\gamma}$  is larger than a critical shear rate are observed. On the microscopic level, one can imagine that the rigid polymers align with the flow at a critical shear rate and concentration. The decrease in viscosity can be described by phenomenological models as, e. g., the power law model  $\eta = k_1 \dot{\gamma}^{(n-1)}$ , which is valid over a given range of shear rates. The value of  $n$  is a measure of the strength of the shear-thinning character of the fluid; for the xanthane solutions, this value ranges from  $n=0.9$  for 50 ppm (parts per million in weight) to  $n=0.46$  for 1000 ppm. For  $n=1$ , the Newtonian limit is recovered. No normal stresses perpendicular to the shear plane can be detected in the tested range of shear rates.

For the flexible polymer PEO, the shear viscosity is nearly constant, whereas significant normal stresses can be detected (see figure 2). With increasing polymer concentration, the Newtonian viscosity increases slightly and the normal stresses become more pronounced. The normal stress is a stress contribution normal to the shear plane in the direction of the velocity gradient. It is, for example, responsible for the Weissenberg effect: if a rod is used to stir a Newtonian liquid in a cup, centrifugal forces depress the surface in a parabolic form. If large normal stresses are present in a viscoelastic fluid, the inverse can be observed and the liquid climbs the rod, as can be observed by stirring the dough. The existence of normal stresses also indicates a strong resistance to elongation; thus, elongational viscosities of fluids that undergo normal stress can be orders of magnitude higher than those of Newtonian fluids. For the dilute and semi-dilute polymer solutions presented here, this viscosity is very difficult to obtain by classical rheology [59].

On a microscopic level, one can imagine coils of the flexible polymer that are stretched by the shearing flow as soon as the shear rate overcomes a critical shear rate, given by the Weissenberg number  $Wi$ . The flow properties of solutions of flexible polymers can be modeled by a microscopic bead and dumbbell model in which a polymer is represented by a spring linking two beads. The dumbbells are convected by the flow. Elastic stretching of the dumbbell due to viscous drag and Brownian forces leads to additional stresses in the flow. By averaging and integrating, a continuum

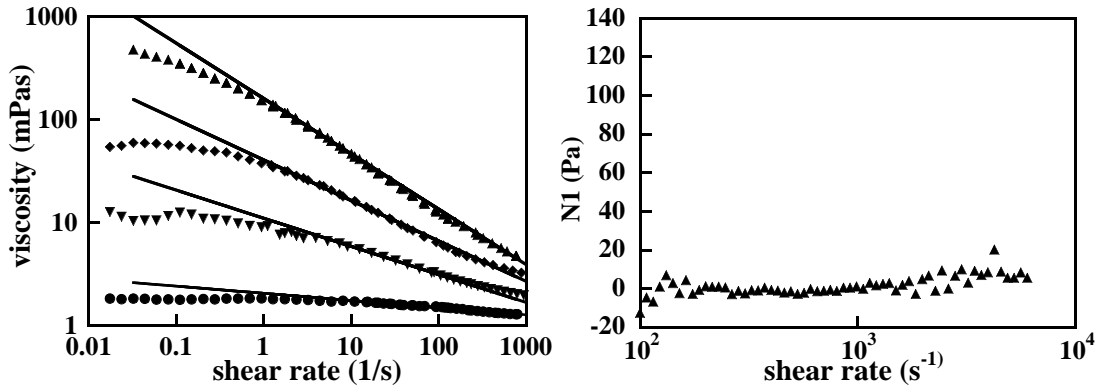


Figure 1: Left) Viscosity  $\eta$  as a function of the shear rate  $\dot{\gamma}$  for different concentrations of xanthane, 50 ppm ( $\bullet$ ), 100 ppm ( $\blacktriangledown$ ), 500 ppm ( $\blacklozenge$ ) and 1000 ppm ( $\blacktriangle$ ). Right) Normal stress  $N_1$  as a function of the shear rate  $\dot{\gamma}$  for a xanthane solution of 1000ppm ( $\blacktriangle$ ).

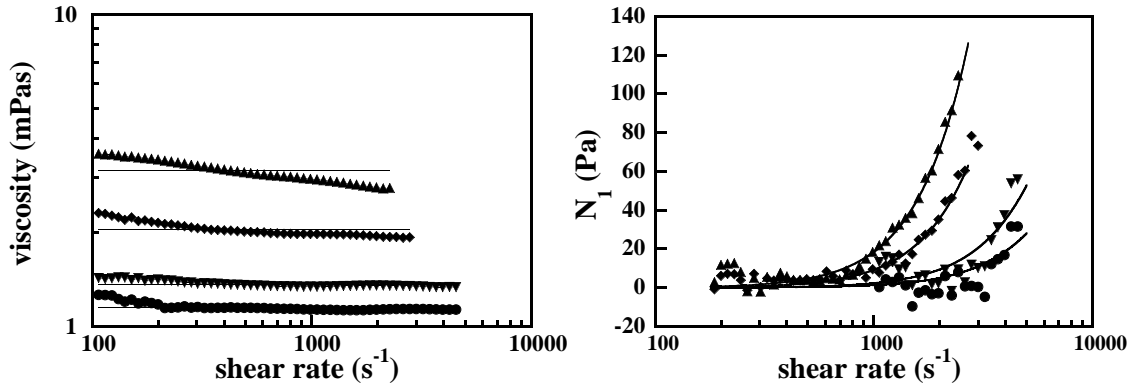


Figure 2: (from [75]) Viscosity  $\eta$  (left) and normal stress  $N_1$  (right) as a function of the shear rate  $\dot{\gamma}$  for solutions of different concentrations of PEO 125 ppm ( $\bullet$ ), 250 ppm ( $\blacktriangledown$ ), 500 ppm ( $\blacklozenge$ ) and 1000 ppm ( $\blacktriangle$ ). The solid lines represent a fit of our data to the prediction of the Oldroyd-B model.

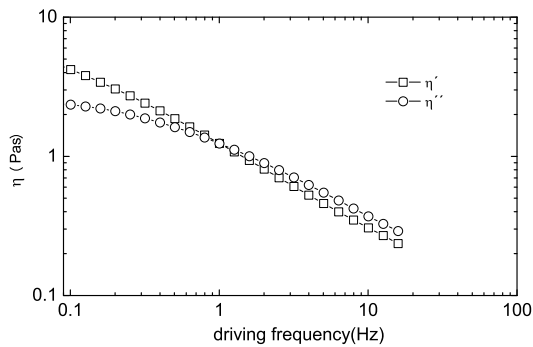


Figure 3: Complex viscosity  $\eta^* = \eta' + i\eta''$  for a 2000 ppm PAA ( $M_w = 4 * 10^6$  g/mol) in 40/60wt% water glycerol solution. The intersection of the dissipative  $\eta''$  and the elastic part  $\eta'$  indicate the inverse relaxation time  $1/\tau_p$  of the liquid.

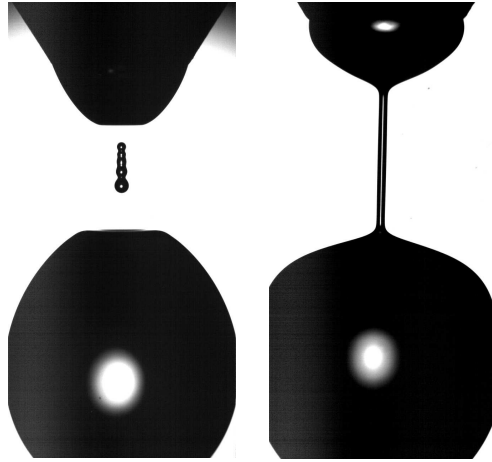


Figure 4: Left image: A droplet of water falling from a nozzle. Right image: The same experiment after the addition of 100ppm PEO ( $M_w = 4 * 10^6$  g/mol).

mechanical model can be obtained. The simplest of these models is the Oldroyd-B model, in which Hookean springs with infinite extensibility are assumed. A first outcome of the Oldroyd-B model is indeed the existence of a normal stress. One finds a constant viscosity and a quadratic increase of the normal stress with shear rate:  $\eta = const$  and  $N_1 = \Psi_1 \dot{\gamma}^2$ . In this model, the viscosity and  $\Psi_1$ , the first normal stress coefficient, are independent from the shear rate and are functions of the polymer relaxation time  $\tau_p$ . On figure 2, one sees that this model fits the experimental data reasonably well. An improved version, the so-called FENE-P model, considers a finite extensibility of the springs and allows description of larger deviations from Newtonian behavior. When used in this manner, the FENE-P model is also valid for higher shear rates or higher elongation rates.

For concentrated solutions of PAA, one can measure a linear elastic response for low deformation. The macroscopic Maxwell model assumes that the stresses in the liquid are given by the sum of a viscous part that is proportional to the shear rate and an elastic part that is proportional to the shear or deformation. The first consequence is that the viscosity becomes a complex number,  $\eta^* = \eta' + i\eta''$ , which has both a dissipative and an elastic part and one can again attribute a characteristic relaxation time,  $\tau_p$ , to the system. The complex viscosity of the solutions as a function of frequency is shown in the figure 3. One can see that even if the complex viscosity cannot be directly fitted with a simple Maxwell model, a relaxation time of  $\tau_p \approx 1$  s can be extracted from the frequency dependency of the complex viscosity at the intersection of the  $\eta'$  and  $\eta''$  curves. Note that the Oldroyd-B model is also referred to as a convected Maxwell model, since for a nonlinear, i.e., finite, deformation, the convection of stress must be taken into account.

### 3. Rayleigh – Plateau instability and droplet pinch-off

#### 3.1. Newtonian liquids

A liquid column with a free surface always disintegrates into smaller droplets because surface tension leads to minimization of the surface-to-volume ratio. Rayleigh showed that the size  $R$  of the droplets is determined by the wave length  $\lambda$  of the sinusoidal distortion with the fastest growth rate. For the inertia-dominated case, i.e., for low viscosity liquids, one finds  $\lambda \approx 9r$  with the radius  $r$  of the column. For the pending droplet, a similar scenario holds. When a pending droplet is fed quasistatically via a syringe pump, it starts to fall if gravitation overcomes capillary forces. However, as soon as the droplet begins to fall, surface tension again leads to minimization of its surface area and acts as the main pinching force [60, 61, 10]. Thus, the primary stages of the pinch-off of a droplet can be modeled as a Rayleigh instability. The thinning dynamics of the neck radius, shown in figure 4, can be fitted with an exponential law corresponding to exponential growth of the amplitude of the most unstable wavelength. The growth rates fit well with the predictions made by Rayleigh's theory [10].

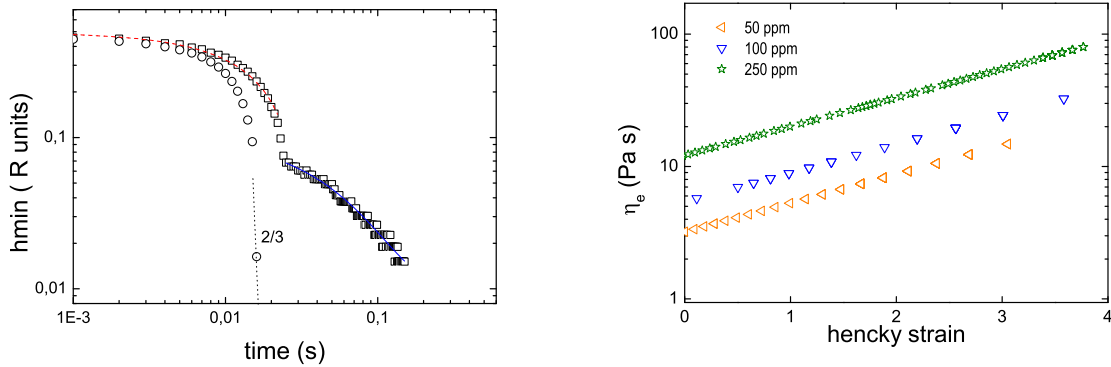


Figure 5: Left) The minimum neck diameter  $h_{min}$  vs. time for water ( $\circ$ ) and 100ppm PEO ( $M_w = 4 * 10^6$  g/mol) in water ( $\square$ ). Dotted line:  $2/3$  power law line as a guide for the eye. Dashed line: exponential fit corresponding to the Rayleigh-Plateau instability of a liquid column of water. Full line: exponential fit in the regime of strongly increasing elongational viscosity. Right) The elongational viscosity for different concentrations of PEO as a function of the Hencky strain.

During the final stages of the pinch-off process in the nonlinear regime, the situation becomes very different. The system no longer reflects the original geometry, e.g., the diameter of the nozzle, but instead depends on material parameters (density, surface tension and viscosity) only. The dynamics of this finite time singularity in which the minimum neck diameter reaches zero in finite time can be described by self-similarity solutions. For the low viscosity and thus inertia-dominated regime, which applies in the case of water, it follows that the minimum neck radius approaches zero such that  $r(t) = 0.7(t - t_c)^{2/3}$  (figure 4) [53].

### 3.2. Polymer solutions

The effect of elasticity on the (linear) dynamics of the Rayleigh-Plateau instability can be best studied theoretically by use of the (linear) Maxwell model. Chang *et al.* [62] performed a linear stability analysis and predicted slight variations of the critical wave numbers and of the growth rates due to linear elasticity.

In the experiments presented here (fig4), solutions of the flexible polymer PEO at low concentrations (10-2000 ppm) in a low viscosity solvent were used. In these solutions, elastic contributions at small deformations are weak and, as a consequence, the complex viscosity  $\eta^*$  is difficult to determine by small amplitude oscillatory shear rheometry. This means that, for small deformation, the polymers do not affect the flow. Indeed, the experimental results (fig5) show that the dynamics of the primary stages of the detachment process are not altered. Only when the flow (and thus the elongation) is strong enough do the polymers become stretched, interrupting the finite time singularity of the pinch-off process. Instead, one observes the formation of a filament and an abrupt transition to a new exponential regime with a much larger time scale. This inhibition of the finite time singularity was first observed by Amarouchene *et al.* [8].

This is a surprising observation because it means that the elastic stresses in the liquid that balance the stresses from the surface tension are much higher than for the case of the pure solvent (fig. 5). Still, the shear viscosity of the sample is close to the solvent viscosity, even at high shear rates. The solution to this apparent contradiction is the following: any type of flow can be divided into a rotational and an elongational part. The elongational part stretches the polymers and induces stresses. The rotational part, e.g., in shear flow, causes the polymers to tumble and stresses are averaged out to a large degree. In the filament, the flow is purely elongational and stretches the polymers most efficiently. This leads to the so-called elongational viscosity  $\eta_e$ . For Newtonian liquids, the elongational viscosity  $\eta_e$  is directly given by geometrical considerations and it follows  $\eta_e = 3\eta_{shear}$ . The factor 3 is called the Trouton ratio. For polymers, the situation is less clear and measurements of the elongational viscosity are non-trivial. The experiment now gives us the opportunity to estimate  $\eta_e$ . In fact, a similar method is used in a commercialized version of the experiment, the so-called CaBER (Capillary Break up Extensional Rheology, Thermo-Fisher Scientific, Karlsruhe, Germany).

Instead of a falling droplet, CaBER uses a capillary bridge formed between two plates that are separated abruptly until the capillary bridge starts to contract. The force balance of the surface stresses and viscous stresses yields an

apparent elongational viscosity  $\eta_e = \frac{\sigma}{r(t)\dot{\epsilon}}$ , with  $\sigma$  the surface tension [63]. Indeed, if the filament is cylindrical, the elongational rate can be obtained via  $\dot{\epsilon} = \frac{\dot{r}(t)}{r(t)}$  and it is constant for the exponential decrease of the radius found in this regime. The minimal neck radius  $r(t)$  shrinks exponentially with time and the elongational viscosity  $\eta_e$  thus increases exponentially with time. This is a type of long-lasting start-up situation in which the increase in stresses holds until the polymers eventually become fully stretched. Fig. 5 shows the elongational viscosity as a function of the Hencky strain  $H$ . The Hencky strain,  $H$ , is a measure of the elongation and is given by  $H = \int \dot{\epsilon} dt$ . The elongational viscosity of the polymer solutions varies from 1 to 100 Pas and is thus five orders of magnitude higher than the shear viscosity (see figure 2).

The growing elastic stresses in the filament stabilize the flow, since any distortions would lead to further stresses. This makes the filament very robust and we might expect a Rayleigh-Plateau-like instability to be observed only at the very end of the thinning process when the polymers are fully stretched and elastic stresses cannot increase further. However, in most of the experiments, a more or less irregular instability scenario is observed at the very end of the thinning process and singular "beads" grow on the filament. In a numerical study, Chang et al [62] predicted that the filament should start to disintegrate from both ends where it is connected to the falling droplet and the reservoir in the nozzle. At these points, the curvature and surface stresses are maximal. These authors predict an iterative disintegration process, similar to the one observed in more viscous Newtonian liquids. Experimentally, Oliveira et al. [64, 65] found an iterative process between generations of larger and smaller beads in a CaBER setup, but their range of observations was limited. Experimental data obtained by Sattler et al. [66] indeed revealed an instability process that was triggered from the ends; instead of an iterative process, we found a Rayleigh-Plateau like instability scenario on the viscoelastic filament. In contrast to previous studies, in which the plates were pulled apart abruptly, in these experiments the separation was performed very gently in order to prevent any additional distortions. Though in most of the experiments singular droplets grew on the filament, it was possible to observe the exponential growth of a coherent sinusoidal pattern, (fig 6 right). The inverse growth rate of the pattern was found to be  $1/\omega = 9.3 \pm 0.1ms$ . Linear stability of a viscous fluid thread [1] predicts  $\omega = \gamma/(6R_0\eta_{eff})$ , resulting in an estimated extensional viscosity of  $\eta_{eff} = 9Pas \pm 2$ , more than one order of magnitude smaller than the extensional viscosity  $\eta_E(12\mu m) = 100Pas$  estimated above, but nevertheless four orders of magnitude higher than the shear viscosity. The exponential regime was followed by the final shrinking of the remaining thread between the beads, which followed a linear law as expected for highly viscous liquids [1, 61].

We must still answer the question of how the filament finally breaks. For polymer concentrations greater than 1000 ppm, it was observed that the liquid filament connecting two beads did not break; instead, a pattern that resembles a solid fiber, as shown in Fig.6 right, a), was formed. The beads sit alongside the filament; experiments on fluid drops on a fiber [67] show that there must be a *finite* contact angle between the drops and the filament for such a symmetry breaking to occur. It follows that the thin filament must have formed a (solid) phase different from that of the drops [68]. This hypothesis could be confirmed by the scanning electron microscopy (SEM) images shown in Fig. 6 right b), in which remnants of two droplets connected by a persistent thin thread are seen. Increased magnification (panels c and d) allowed us to estimate the diameter of the fiber as  $75 - 150nm$ . Our interpretation of this data is that, due to the coupling of stress fluctuations and concentration fluctuations, a flow-driven phase separation takes place. Microscopically, one can imagine that while solvent drains from the filament, the polymers become entangled, leading to even higher polymer concentration and increased entanglement, i.e., flow-induced phase separation takes place [69]. Further evidence for this concentration process was found in [70], where birefringence measurements were performed to examine molecular conformations in the break-up process. Evaporation can be excluded as a factor in the formation of solid fibers, based on experiments in a two-fluid system.

## 4. Saffmann – Taylor

### 4.1. The classical Saffman – Taylor instability

The classical Saffman-Taylor instability occurs when, for example, air pushes a viscous fluid in a narrow channel of height  $b$  and width  $W$ , a so called Hele-Shaw cell. In the following, the viscosity of air is neglected and the viscosity of the viscous liquid is given by  $\eta$ . The surface tension between the two fluids is  $\sigma$  and the viscous liquid is considered to perfectly wet the channel.

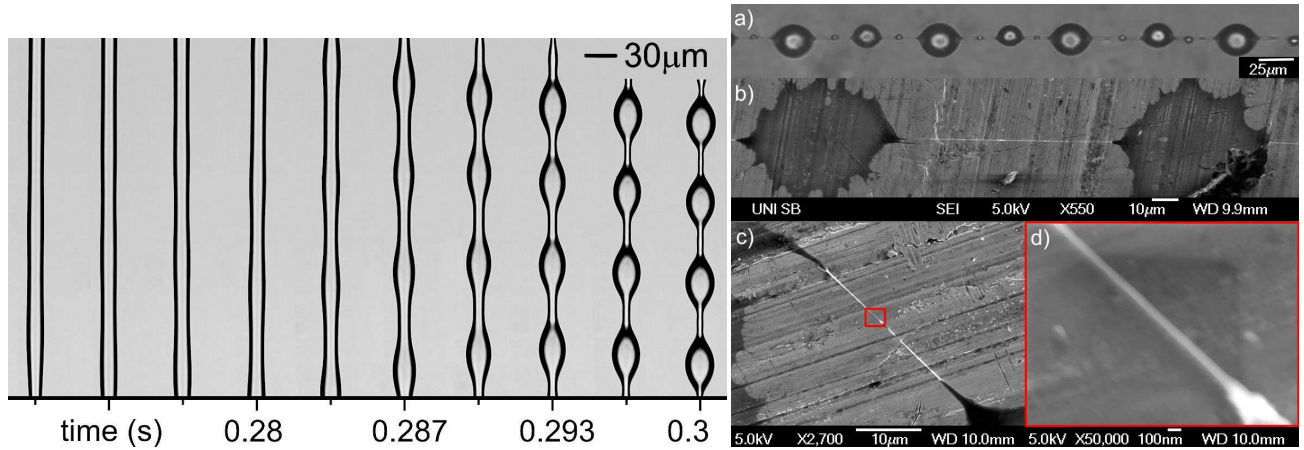


Figure 6: Left) (Fig. 2 from [66]) Growth of a sinusoidal instability of the viscoelastic filament of an aqueous PEO solution (1000 ppm) that develops into a group of droplets on the thinning filament. The spacing of the pictures is 1/300 s. Right) (Fig. 4 from [66]) a) The final state of the filament. Beads are formed off-center relative to the thread. b) Scanning electron microscopy image of two beads connected by a thread (intermediate resolution). The structure was caught and dried upon the substrate. c) Another example of the structure; the red box indicates a closeup at high magnification shown in d). The diameter of the fiber can be as small as 70nm.

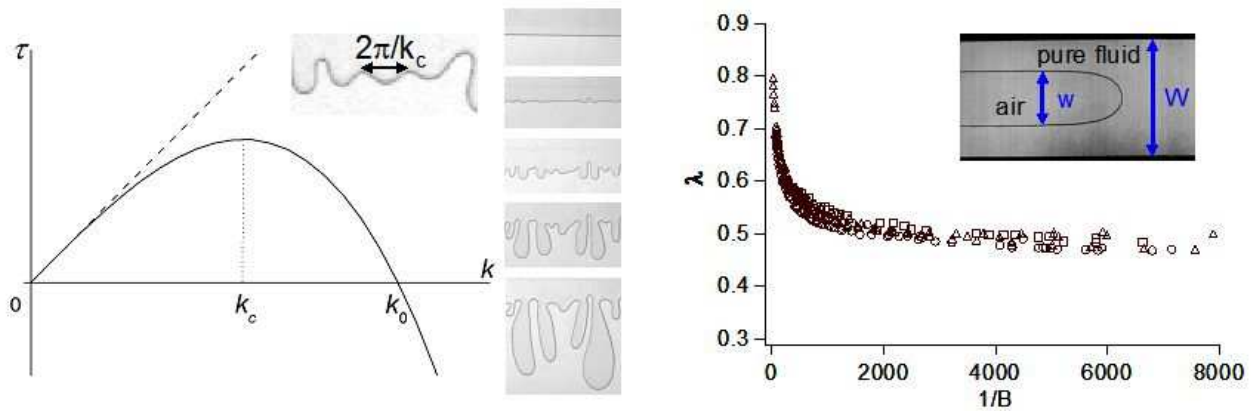


Figure 7: Left) Growth rate  $\tau$  as a function of the wave number  $k$ . The most unstable wavelength  $l_c$  is given by  $2\pi/k_c$ . Inset: Snapshots of the destabilization of a planar front between air and silicon oil (courtesy D. Derks and A. Lindner). Right) relative finger width  $\lambda$  as a function of the control parameter  $1/B$  for air pushing silicon oils of different viscosities in channels of different geometries. Inset: snapshot of a finger advancing into a linear cell (courtesy C. Chevalier).

Flow in the confined geometry is then governed by Darcy's law, which gives the mean velocity (averaged over the thickness of the channel) of the fluid as a function of an applied pressure gradient :  $\mathbf{V} = -\frac{b}{12\eta}\nabla p$ . The incompressibility of the fluid reads  $\nabla \cdot \mathbf{V} = 0$  and one thus deals with growth in a Laplacian pressure field  $\Delta p = 0$ . The pressure jump at the interface is given by  $\delta p = \sigma \left( \frac{2}{b} + \kappa \right)$ , with  $\kappa$  being the curvature in the direction of the channel width, once again using a two-dimensional approximation. Together with the boundary conditions, this set of equations completely determines the problem.

When the less viscous fluid pushes the more viscous fluid, an initially straight interface becomes unstable. Small perturbations lead to an increased pressure gradient and a higher velocity in front of the perturbations and are thus amplified. Surface tension, on the other hand, stabilizes the initially straight interface. The competition between viscous and capillary forces leads to the emergence of a characteristic length scale that can be calculated using linear stability analysis [71]. The maximum growth rate is found for a wavelength  $l_c = \pi b / \sqrt{Ca}$  with capillary number  $Ca = \eta U / \sigma$ . The small fingers grow and begin to compete with the more advanced fingers, screening the less advanced fingers. In a linear channel of width  $W$ , one finally observes a single finger propagating through the cell, the result of a non-linear growth process. An example of initial finger growth and finger competition, together with the growth rate obtained from the linear stability analysis, can be seen in figure 7a. The relative width of the single finger  $\lambda$ , defined as the ratio between the finger width  $w$  and the cell width  $W$ , is given by the control parameter  $1/B = 12Ca(W/b)^2$ ; that is, the ratio between the two length scales of the system  $W$  and  $l_c$ . Representation of the results obtained using different fluids (and thus different surface tensions or different viscosities) and different cell geometries as a function of the control parameter  $1/B$  shows that the results fall on a universal curve (see figure 7b). With increasing velocity  $U$  of the finger tip, viscous forces become increasingly important compared to capillary forces and the relative finger width decreases. At high velocity, the finger width does not, however, tend to zero but stabilizes near a plateau value at  $\lambda = 0.5$ .

This instability was described by Saffman and Taylor [29] in 1958; however, finger selection remained a puzzle for several decades. Neglecting surface tension, Saffman and Taylor found a family of analytical solutions of the shape of the interface given by  $x = \frac{W(1-\lambda)}{2\pi} \ln \left[ \frac{1}{2} \left( 1 + \cos \frac{2\pi y}{\lambda W} \right) \right]$  that agrees well with experimental observations. This treatment does not, however, explain the selection of a given finger width. For this, one must take the surface tension into account. This was done numerically by McLean and Saffman in 1981 [54]. The selection process was solved analytically only much later [55, 56, 57] and was attributed to the fact that the surface tension represents a singular perturbation leading to a solvability condition at the finger tip. It is this condition that selects the finger from the family of solutions found by Saffman and Taylor.

So far, we have treated an ideal two-dimensional problem. In reality, however, there is a thin wetting film that remains between the advancing finger and the glass plates. The thickness of this film, according to the Bretherton law, is proportional to  $Ca^{2/3} t/R = 0.643(3Ca)^{2/3}$  [72]. As a consequence, the pressure jump at the interface is continuously modified. This three-dimensional effect leads to the slight modification of the finger width observed between different experimental geometries, as observed in figure 7.

#### 4.2. Finger narrowing in shear thinning fluids

When performing experiments in dilute solutions of xanthane, one observes a strong modification of the selection process. As can be seen in the snapshot in Figure 8a, at high velocity, fingers are found to be significantly narrower than the classical limit of  $\lambda = 0.5$ . This observation can be qualitatively linked to the behavior of the shear thinning fluid pushed by the finger in the Hele-Shaw cell. Numerical simulations [73, 74] show that the viscosity is not uniform throughout the cell (see figure 8b); regions of high fluid velocity and thus high shear rate have a low viscosity. This is essentially the case in front of the finger tip and the system becomes anisotropic, leading to finger narrowing.

For weak shear thinning ( $1 > n > 0.65$ ), we have shown [75, 36] that simply replacing in the control parameter  $1/B$  the constant viscosity  $\eta$  by a shear-dependent viscosity  $\eta(\dot{\gamma})$  allows rescaling the data onto the universal curve for Newtonian fluids. The shear rate  $\dot{\gamma}$  is here the average shear rate in the cell. For stronger shear-thinning ( $n < 0.65$ ), this rescaling fails and deviations from the classical result toward smaller fingers are observed.

Narrower fingers have also been observed by Rabaud *et al.* [76]. Using a Hele – Shaw cell with engraved glass plates, they found viscous fingers with  $\lambda$  significantly smaller than 0.5 for Newtonian fluids. The observation of such "anomalous" fingers is explained by the fact that the engravings represent a local perturbation at the finger tip. This disturbance removes the classical selection of the discrete set of solutions. The continuum of solutions given by the

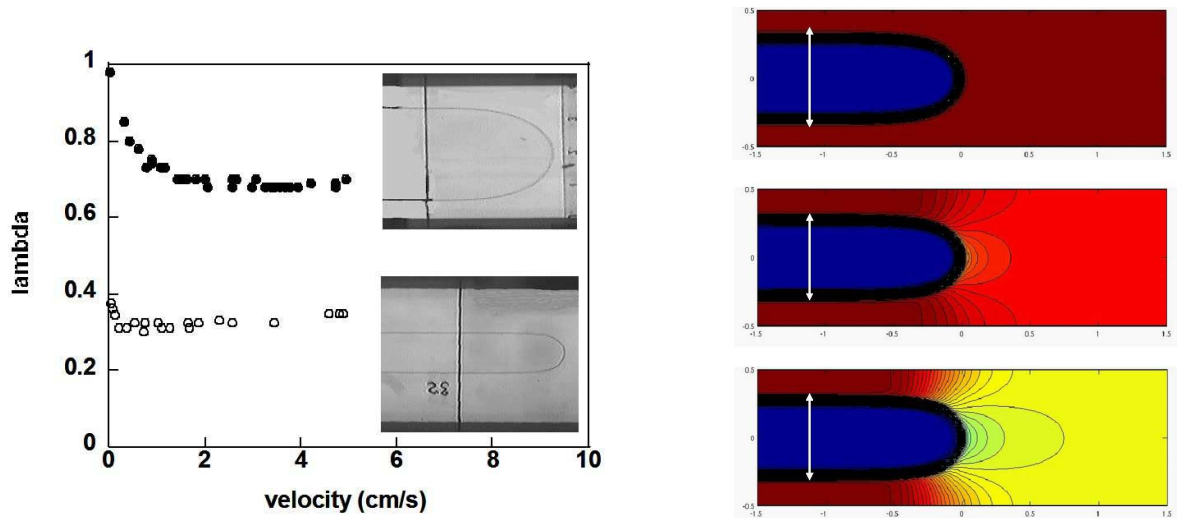


Figure 8: Left) Relative finger width  $\lambda$  as a function of the velocity  $v$  for solutions of xanthane ( $\circ$ ) at 1000 ppm and PEO ( $\bullet$ ) at 50 ppm. Inset: snapshots of fingers in the two solutions at high velocity (4 cm/s). Right) Viscosity in front of the advancing finger in a shear thinning fluid found from numerical simulations [73]. The shear thinning effect increases from top to bottom. Red corresponds to high viscosities and yellow to low viscosities.

analytical result of Saffman and Taylor without surface tension then becomes accessible:  $\lambda$  can take values smaller than 0.5 at high velocity. Rabaud *et al.* showed that for a given value of the capillary number  $Ca$ , it is not the relative finger width that is selected but that the dimensionless radius of curvature at the tip  $\rho/b$ .  $\rho$  can be linked to the finger width  $\lambda$  via the relation  $\rho = \frac{\lambda^2 W}{\pi(1-\lambda)}$ , which follows from the finger shape predicted by Saffman and Taylor.

A similar mechanism has been found to be responsible for the selection of the viscous fingers in a shear thinning fluid. Here when the shear thinning character of the fluid is strong enough, anisotropy plays the role of the perturbation at the finger tip. Figure 9a shows experimental finger profiles for a given capillary number and three different cell widths. One clearly observes that the radius at the finger tip is identical for the three experiments, leading to lower finger width compared to the Newtonian case, in which the relative finger width  $\lambda$  is selected. The relation between  $\rho/b$  and  $\lambda$  is found to depend on the shear thinning character of the fluids and thus the shear thinning exponent  $n$ . Knowledge of the relationship between  $\rho/b$  and  $\lambda$  solves the selection problem, as we can now predict the finger width  $\lambda$  from the rheological data. The presence of shear thinning thus leads to a completely different selection mechanism that is closer to what is observed, for example, in dendritic growth [30] and which requires anisotropy in the system. Corvera Poiré *et al.* [77] directly solved the problem for a power law fluid; their results are in good agreement with the experimental observations. Note that at high velocities one observes a saturation of  $\rho$ , leading to an increase of the finger widths. This might be attributed to inertial effects, which have been observed to increase finger width [43] and which may begin to play a role in this low viscosity fluid.

#### 4.3. Finger widening due to normal stresses

In experiments using solutions of the flexible polymer PEO, completely different behavior is found. In contrast to the observations in shear thinning fluids, where finger narrowing occurs, one now observes finger widening compared to the Newtonian case (see figure 8a).

The presence of normal stresses in the thin wetting layer might be responsible for the finger widening; one can attempt to account for this effect by adding a supplementary pressure to the system. In classical theory, the pressure jump at the interface between two liquids is given by the radius of curvature. Tabeling *et al.* [72] have shown that one can incorporate the effect of a finite thickness of the wetting film by correcting the surface tension in the control parameter. Following the same argument, in the control parameter one can add the supplementary pressure caused by the normal stresses to the surface tension term  $\sigma^* = \sigma + 1/2N_1(\dot{\gamma})b$ . For moderate normal stresses, this allows rescaling of the data onto one universal curve and once again solves the selection problem.

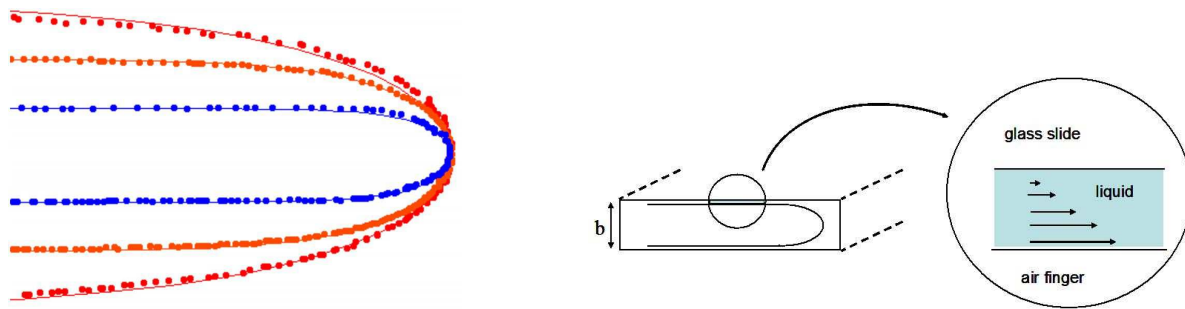


Figure 9: Left) Experimental finger shapes in a solution of xanthane of 2000 ppm for three different channel widths  $W=2, 4,$  and  $8$  cm. Right) Sketch of the thin wetting layer observed between the finger and the glass plates

## 5. Faraday instability

### 5.1. History

The Faraday experiment was first reported in 1831 [16]. In an appendix of a paper on Chladni figures, Faraday reports on the crisped state of a layer of liquid that is shaken vertically. He refers to works by "*Oersted, Wheatstone and Weber and probably others (sic)*" who had earlier mentioned the phenomenon; however, according to Faraday, it was he who gave the first conclusive description. The experimental setup consisted of a box that was mounted on a rod. The rod was set into vibration by a bow; its oscillation frequency was presumably on the order of a few Hz. When the oscillation amplitude exceeded a certain critical value, standing capillary surface waves were observed. Apparently, Faraday was impressed by the richness of the patterns and noted: "*obtained in this way the appearances were very beautiful, and the facilities very great*". It is a remarkable achievement that even at that early date Faraday found that the surface waves oscillate with half of the driving frequency. This is the so-called subharmonic response. Faraday also pointed out differences in the wavy surface patterns when he compared simple oils with, e.g., the white of an egg. He stated: "*The difference between oil and white of egg is remarkable; . . . the crisped state may be a useful and even important indication of the internal constitution of different fluids.*"

In 1868, Matthiesen [78] reported on systematic measurements; he stated incorrectly that the surface response should be synchronous to the drive. In 1883, Lord Rayleigh [79] proposed a theoretical treatment in terms of a parametric pendulum, the Mathieu oscillator. In 1954, Benjamin and Ursell [80] solved the linear problem for ideal liquids (without viscosity) with an infinite set of Mathieu oscillators that oscillate with integral and  $(n + 1)/2$  multiples of the driving frequency. The integral multiples correspond to a possible harmonic (synchronous) response and the  $(n + 1)/2$  to a subharmonic response (figure 10). In 1994, Kumar and Tuckermann [81] presented a numerical analysis of the linear problem in the case of viscous liquids with finite depth of the layer. Together with an analytical treatment, this analysis was used to find parameters to experimentally reproduce a harmonic response using a very thin layer of liquid [82]. Recently, a large variety of patterns with up to 10-fold rotational symmetry (quasiperiodic), superlattices or localized patterns have been reported [20, 19, 83]. A variety of these patterns could be obtained using a simple liquid driven with a single frequency. Near onset, in linear order, a single wave number first became unstable. The resulting wave vector(s) could have any orientation, but nonlinear interaction with the higher harmonics led to a given pattern selection process [17, 82, 84]. Obviously, the pattern dynamic might become even richer if *two* discrete wave numbers become unstable simultaneously.

It is worth mentioning that numerical simulation of the full hydrodynamical problem of the Faraday experiment with a single driving frequency for simple liquids became available only very recently [52]. Périnet *et al.* solved the complete nonlinear Navier – Stokes equations by a finite-difference projection method coupled to a Front Tracking technique for the calculation of the surface tension forces and advection of the interface. They compared the complete spatial and temporal Fourier spectrum of the surface state and found good agreement with experimental data from Kityk *et al.* [85]. A quantitative theoretical description of the nonlinear wave state of complex liquids remains an even more challenging problem that is still unsolved.

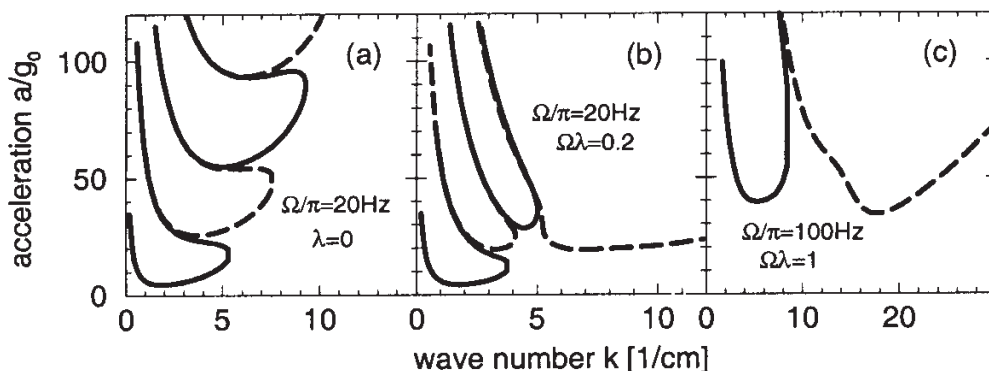


Figure 10: (From [27]) The linear stability diagram of the Faraday experiment for a Maxwell fluid. Full lines mark the transition to the subharmonic response and dashed lines to the harmonic one. a) For a Newtonian fluid, i.e., when the polymer relaxation time  $\tau_p$  is zero, the subharmonic response becomes unstable first. b) For finite relaxation times, a new harmonic tongue appears c) Only when the inverse polymer relaxation time compares to the driving angular frequency  $\Omega$  does the new harmonic instability tongue become unstable first.

## 5.2. Complex liquids

The first experimental data on Faraday waves of polymer solutions were, to our knowledge, presented in 1998 by Raynal, Kumar and Fauve [23]. Their work concentrates on *dilute* polymer solutions where the influence of elasticity is small. They found a slight shift of the critical acceleration; the critical wave numbers were not affected. In 1999, Müller and Zimmermann presented a linear stability analysis for a Maxwell fluid [27]. They found that when the inverse of the relaxation time of the Maxwell fluid compares to the driving frequency, a harmonic response might become unstable first and that, for a certain set of parameters, a bistable situation exists; see fig. 10. Again, in 1999, Wagner and Müller presented experimental and theoretical data on a Faraday experiment using a concentrated polymer solution of 2000 ppm PAA ( $M_w = 4 * 10^6$  g/mol) in a water-glycerol mixture [24] with a relaxation time  $\tau_p \sim 1$  s (see section 2). The rheological data obtained for the complex viscosity was then fed into the linear stability algorithm of Kumar and Tuckerman [81] and a reasonable agreement of the experimentally and numerically determined critical accelerations was obtained. Notably, a bicritical situation was found in which the subharmonic and harmonic responses became unstable simultaneously.

In fig. 11, an overview of the observed patterns is presented. This phase diagram was obtained by setting a fixed frequency and varying the driving strengths. When a (new) pattern was visible, the transition point was noted. The primary instability was found to be hysteretic ( $\epsilon < 0$ ) and most of the transitions between the patterns were hysteretic as well (not shown). For frequencies well above the bicritical frequency  $f_b \approx 39\text{Hz}$ , a subharmonic pattern of lines (region V) was observed corresponding to observations in a Newtonian liquid of similar viscosity. For parameters where only a harmonic response existed, a coherent pattern of hexagons was observed (region IIa, fig. 12a). The hexagonal symmetry is generic for a harmonic response where the temporal symmetry allows the coupling of three wave vectors  $H_n$  that are equally distributed on the critical circle (fig.12c). For frequencies close to the bicritical point, with increasing driving strength subharmonic wave vectors  $S_n$  also become unstable. They are slaved by the harmonic hexagonal pattern and arrange together to a  $2 \times 2$  superlattice. The nomenclature is taken from crystallography and relates to the ratio of 1 : 2 of the harmonic and subharmonic wave vectors, which is close to the ratio of linear unstable wave numbers (region IIIa, fig. 12b).

The pattern-forming process can be understood in the following way. The linear stability analysis reveals that the surface state consists of a singular wave number  $k$  (only exactly at the bicritical point do two wave modes synchronously become unstable) but of an infinite series of temporal Fourier components,  $n\Omega$  or  $(n + 1)/2\Omega$  for the harmonic or subharmonic responses, respectively. This linear result is fed into the nonlinear equations for the hydrodynamic velocity field  $\mathbf{v}$ . The solvability condition in quadratic order implies that resonant terms must vanish in the higher orders to prevent secular growth. For the temporal components, an arbitrary quadratic nonlinearity results in

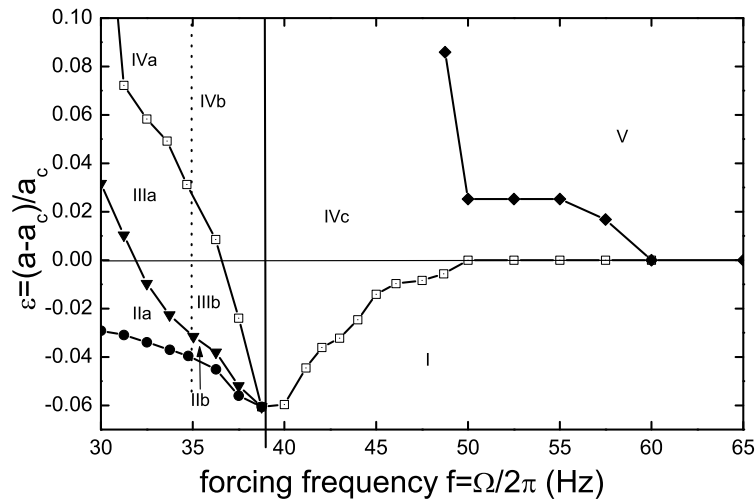


Figure 11: (Fig. 2 from [24]) Phase diagram of the observed nonlinear patterns. The symbols mark experimental data points. The abscissa,  $\epsilon = \frac{a - a_c}{a_c} = 0$ , indicates the linear threshold with  $a$  the acceleration amplitude and  $a_c$  the critical acceleration. The lowest solid line denotes the saddle point of the hysteresis. Region I: flat surface; IIa: harmonic hexagons covering the whole surface; IIIa: harmonic-subharmonic hexagonal superlattice (see text) extending over the whole surface; IIb, IIIb: as before, but patterns occur in the form of localized patches surrounded by the flat surface; IVa, IVb, IVc: chaotic dynamics of subharmonic lines competing with extended (a) or localized (b) hexagonal superlattices or the flat surface (c); V: stationary subharmonic lines extending over the whole surface (Newtonian regime).

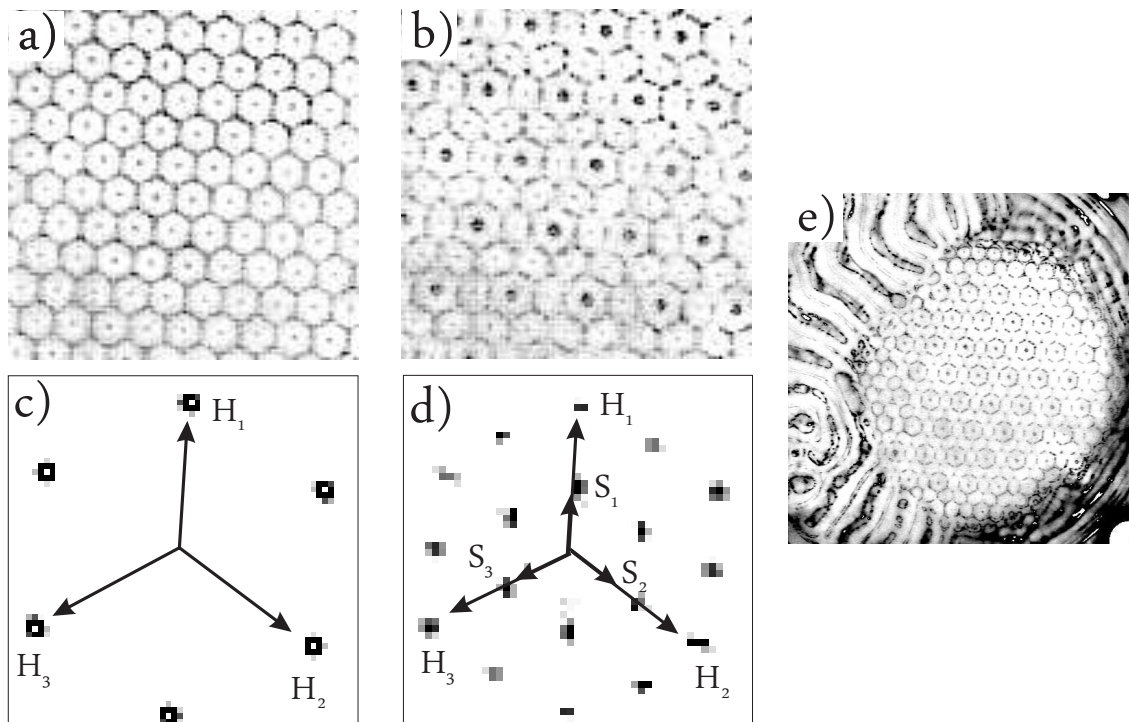


Figure 12: (a) The harmonic hexagonal pattern. (b) the harmonic-subharmonic hexagonal superlattice. (c) and (d) the respective spatial Fourier spectra. (e) (Fig. 4 from [24]) Localized stationary surface patterns of harmonic hexagons in coexistence with a localized nonstationary patch of lines.

a frequency spectrum of integral multiples of  $\Omega$ , whether or not S or H are considered. Thus, quadratic nonlinearities are able to resonate with *harmonic* linear eigenmodes, but not with *subharmonic* ones. In the same way, spatial resonance must be guaranteed as well. Now, any triplet of harmonic modes  $\{\mathbf{k}_{H1}, \mathbf{k}_{H2}, \mathbf{k}_{H3}\}$  with  $|\mathbf{k}_{Hm}| = k_H$  and  $\mathbf{k}_{H1} + \mathbf{k}_{H2} + \mathbf{k}_{H3} = 0$  are in resonance. This generic 3-wave vector coupling is well known (e.g., from non-Boussinesq-Rayleigh-Bénard convection) and enforces a saddle node bifurcation towards hexagonal patterns. The associated solvability condition is referred to as the amplitude equation or Ginzburg–Landau equation. Within the subharmonic regime, such a resonant 3-wave vector coupling is prohibited due to the missing temporal resonance. The pattern selection mechanism is therefore then controlled by the cubic coupling coefficient in the associated amplitude equations [84, 86], and a variety of patterns is allowed.

The secondary superstructure must result from a nonlinear excitation process, as well. The responsible mechanism is again a 3-wave vector interaction. The linear analysis yields the result that the wave number of the subharmonic response is approximately  $|\mathbf{k}_{S1}| = \frac{1}{2}|\mathbf{k}_{H1}|$ . Invoking basic resonance arguments, one finds directly  $\mathbf{k}_{S1} = \frac{1}{2}\mathbf{k}_{H1}$ .

For increased driving strength, localized patches of hexagons have also been observed. They cannot be explained by a triplet of real Landau equations supplemented by diffusive spatial derivatives, since within this familiar amplitude equation model, *stable* isolated islands of hexagons do not exist. For even larger driving strength, the patterns become chaotically time-dependent. Patches of subharmonically oscillating lines originating in an erratic manner from the cell boundary or the flat surface penetrate into the stationary hexagonal superlattice. They then disappear and the original structure is recovered. This process repeats itself on time scales of seconds to minutes, leading to a temporary coexistence of the stationary hexagonal superlattice with subharmonic lines (region *IVb*, fig. 12). Higher driving amplitudes lead to a fully chaotic surface pattern. Still, no satisfying theoretical description of these states exists.

## 6. Summary

In the present paper, we have revisited three classical surface instabilities, the Rayleigh–Plateau instability followed by the detachment of a droplet, the Saffman–Taylor instability and the Faraday experiment. We have described the modifications of the selection processes that occur when polymer solutions instead of simple Newtonian fluids are used. We have shown that the non-Newtonian properties that come into play when using viscoelastic fluids can fundamentally modify the selection processes. The Rayleigh–Plateau instability, which describes the onset of the detachment of a droplet, is not modified by the use of dilute solutions of a flexible polymer, as the linear viscoelastic properties of this solution are weak. The final detachment of the droplet is, however, strongly delayed as high stresses develop when the fluid filament becomes more and more stretched. The additional resistance to breakup can be attributed to large elongational viscosities present in these solutions. Only in the final stages of the detachment process, when the polymers are fully stretched, might another Rayleigh–Plateau instability be observed. Eventually, a flow-induced phase separation may lead to a solid nanofiber. Using this type of polymer solution also leads to a modification of the Saffman–Taylor or viscous fingering instability. Normal stresses develop in the thin wetting film left between the advancing finger and the glass plates of a Hele–Shaw cell, leading to finger widening compared to the classical results. When using shear thinning solutions of a rigid polymer, finger narrowing is observed. This can be attributed to an anisotropy that develops in the system. In front of the finger tip, where the shear rate is high, the viscosity is decreased. For strong shear thinning, the selection process is quantitatively modified as the anisotropy removes the solvability condition at the finger tip that is responsible for the selection process in Newtonian fluids. The selection process resulting from this anisotropy is found to be closer to that involved in the formation of dendrites. The Faraday instability is studied in a concentrated polymer solution that can be approximately described by a Maxwell model. It has been shown that when the relaxation time of the complex fluid is of the same order of magnitude as the driving frequency, a subharmonic and an harmonic response can become unstable simultaneously. This leads to an entirely new class of patterns, the so-called superlattices.

## A. Acknowledgements

We thank Julia Nase for a critical reading of the manuscript.

## References

- [1] J. Eggers, Nonlinear dynamics and breakup of free-surface flows, *Rev. Mod. Phys.* 69 (1997) 865-929.
- [2] J. Eggers, E. Villermaux, Physics of liquid jets, *Rep. Prog. Phys.* 71 (2008) 036601.
- [3] M. Goldin, J. Yerushal, R. Pfeffer, R. Shinnar, Breakup of a laminar jet of a viscoelastic fluid, *J. Fluid Mech.* 38 (1969) 689.
- [4] A. Bazilevskii, S. Voronkov, V. Entov, A. Rozkhov, On orientational effects of jets and threats of dilute polymer solutions, *Dokl. Akad. Nauk SSSR* 257 (1981) 336-339.
- [5] M. Renardy, How to integrate the upper convected Maxwell (UCM) stress near a singularity (and maybe elsewhere, too), *J. Non-Newtonian Fluid Mech.* 52 (1994) 91-95.
- [6] Entov, V.M. and Hinch, E.J., Effect of a Spectrum of Relaxation Times on the Capillary Thinning of a Filament of Elastic Liquid, *J. Non-Newt. Fluid Mech.* 72 (1997) 31-54.
- [7] M. Stelter, G. Brenn, A.L. Yarin, R.P. Singh, F. Durst, Validation and application of a novel elongational device for polymer solutions, *J. Rheol.* 44 (2000) 595616.
- [8] Y. Amarouchene, D. Bonn, J. Meunier, H. Kellay, Inhibition of the finite-time singularity during droplet fission of a polymeric fluid, *Phys. Rev. Lett.* 86 (2001) 3558-3561.
- [9] S. Anna, G. McKinley, Elasto-capillary thinning and breakup of model elastic liquids, *J. Rheol.* 45 (2001) 115-138.
- [10] C. Wagner, Y. Amarouchene, D. Bonn, J. Eggers, Droplet detachment and satellite bead formation in viscoelastic fluids, *Phys. Rev. Lett.* 95 (2005) 164504.
- [11] V. Tirtaatmadja, G. McKinley, J. Cooper-White, Drop formation and breakup of low viscosity elastic fluids: Effects of molecular weight and concentration, *Phys. Fluids* 18 (2006) 043101.
- [12] C. Clasen, J. Eggers, M. Fontelos, J. Li, G. McKinley, The beads-on-string structure of viscoelastic threads, *J. Fluid Mech.* 556 (2006) 283-308.
- [13] P. Coussot, F. Gaulard, Gravity flow instability of viscoplastic materials: The ketchup drip, *Phys. Rev. E* 72 (2005) 031409.
- [14] Katarzyna Niedzwiedz, Oliver Arnolds, Norbert willenbacher, Rudiger Brummer, Capillary Breakup Extensional Rheometry of Yield Stress Fluids, *Appl. Rheol.* 19 (2009) 41969.
- [15] R. J. Furbank, J. F. Morris, Pendant drop thread dynamics of particle-laden liquids, *Int. J. Multiphase Flow* 33 (2007) 448-468.
- [16] M. Faraday, On the forms and states of fluids on vibrating elastic surfaces, *Philos. Trans. R. Soc. London* 52 (1831) 319.
- [17] W. Zhang, J. Vinals, Square patterns and quasipatterns in weakly damped Faraday waves, *Phys. Rev. E* 53 (1996) R4283-R4286.
- [18] O. Lioubashevski, H. Arbell, J. Fineberg, Dissipative solitary states in driven surface waves, *Phys. Rev. Lett.* 76 (1996) 3959-3962.
- [19] D. Binks, W. vandeWater, Nonlinear pattern formation of Faraday waves, *Phys. Rev. Lett.* 78 (1997) 4043-4046.
- [20] A. Kudrolli, B. Pier, J. Gollub, Superlattice patterns in surface waves, *Physica D* 123 (1998) 99-111.
- [21] C. Wagner, H. Müller, K. Knorr, Crossover from a square to a hexagonal pattern in Faraday surface waves, *Phys. Rev. E* 62 (2000) R33-R36.
- [22] P. B. Umbanhowar, F. Melo, H. L. Swinney, Localized excitations in a vertically vibrated granular layer, *Nature* 382 (1996) 793-796.
- [23] F. Raynal, S. Kumar, S. Fauve, Faraday instability with a polymer solution, *Eur. Phys. J. B* 9 (1999) 175-178.
- [24] C. Wagner, H. Müller, K. Knorr, Faraday waves on a viscoelastic liquid, *Phys. Rev. Lett.* 83 (1999) 308-311.
- [25] P. Ballesta, S. Manneville, Signature of elasticity in the Faraday instability, *Phys. Rev. E* 71 (2005) 026308.
- [26] A. V. Kityk, C. Wagner, Delay of disorder by diluted polymers, *Europhys. Lett.* 75 (2006) 441-447.
- [27] H. Müller, W. Zimmermann, Faraday instability in a linear viscoelastic fluid, *Europhys. Lett.* 45 (1999) 169-174.
- [28] F. S. Merkt, R. D. Deegan, D. I. Goldman, E. Rericha, H. L. Swinney, Persistent holes in a fluid, *Phys. Rev. Lett.* 92 (2004) 184501.
- [29] P. Saffman, G. Taylor, The penetration of a fluid into a porous medium or hele-shaw cell containing a more viscous liquid, *Proc. R. Soc. A* 245 (1958) 312-329.
- [30] Y. Couder, Viscous fingering as an archetype for growth patterns, in: G. Batchelor, H. Moffat, M. Worsert (Eds.), *Perspectives in Fluid Dynamics*, Cambridge University Press, Cambridge, 2000, pp. 53-104.
- [31] Y. Couder, Growth patterns: from stable curved fronts to fractal structures, in: Artuso et. al. (Ed.), *Chaos, order and patterns*, Plenum press, New York, 1991, pp. 203-227.
- [32] G. Homsy, Viscous fingering in porous media, *Ann. Rev. Fluid Mech.* 19 (1987) 271-311.
- [33] D. Bensimon, L. Kadanoff, S. Liang, B. Shraiman, C. Tang, Viscous flows in two dimensions, *Rev. Mod. Phys.* 58 (1986) 977-999.
- [34] K. McCloud, J. Maher, Experimental perturbations to Saffman-Taylor flow, *Phys. Rep.* 260 (1995) 139-185.
- [35] H. VanDamme, Flow and interfacial instabilities in newtonian and colloidal fluids (or the birth, life and death of a fractal), in: D. Avnir (Ed.), *The Fractal Approach to Heterogeneous Chemistry*, John Wiley and Sons Ltd., 1989.
- [36] A. Lindner, D. Bonn, E. C. Poire, M. Ben Amar, J. Meunier, Viscous fingering in non-newtonian fluids, *J. Fluid Mech.* 469 (2002) 237-256.
- [37] H. Zhao, J. Maher, Associating-polymer effects in a hele-shaw experiment, *Phys. Rev. E* 47 (1993) 4278-4283.
- [38] Greffier, O. and AlKawaji, A. and Rouch, J. and Kellay, H., Observation of Finite-Time Singularity in Needle Propagation in Hele-Shaw Cells, *Phys. Rev. Lett.* 81 (1998) 3860-3863
- [39] D. Bonn, H. Kellay, M. BenAmar, J. Meunier, Viscous finger widening with surfactants and polymers, *Phys. Rev. Lett.* 75 (1995) 2132-2135.
- [40] A. Lindner, P. Coussot, D. Bonn, Viscous fingering in a yield stress fluid, *Phys. Rev. Lett.* 85 (2000) 314-317.
- [41] N. Puff, G. Debregas, J.-M. d. Meglio, D. Higgins, D. Bonn, C. Wagner, Stick-slip instability for viscous fingering in a gel, *Europhys. Lett.* 58 (2002) 524-529.
- [42] S. Park, D. Durian, Viscous and elastic fingering instabilities in foam, *Phys. Rev. Lett.* 72 (1994) 3347-3350.
- [43] C. Chevalier, M. Ben Amar, D. Bonn, A. Lindner, Inertial effects on Saffman-Taylor viscous fingering, *J. Fluid Mech.* 552 (2006) 83-97.
- [44] C. Chevalier, A. Lindner, M. Leroux, E. Clement, Morphodynamics during air injection into a confined granular suspension, *J. Non-Newtonian Fluid Mech.* 158 (2009) 63-72.
- [45] O. Johnsen, C. Chevalier, A. Lindner, R. Toussaint, E. Clement, K. J. Maloy, E. G. Flekkoy, J. Schmittbuhl, Decomposition and fluidization of a saturated and confined granular medium by injection of a viscous liquid or gas, *Phys. Rev. E* 78 (2008) 051302.

- [46] X. Cheng, L. Xu, A. Patterson, H. M. Jaeger, S. R. Nagel, Towards the zero-surface-tension limit in granular fingering instability, *Nat. Phys.* 4 (2008) 234-237.
- [47] J. Nase, A. Lindner, C. Creton, Pattern formation during deformation of a confined viscoelastic layer: From a viscous liquid to a soft elastic solid, *Phys. Rev. Lett.* 101 (2008) 074503.
- [48] A. Gupta, Stability of a visco-elastic liquid film flowing down an inclined plane, *J. Fluid Mech.* 28 (Part 1) (1967) 17-76.
- [49] J. P. Tordella, Fracture in the Extrusion of Amorphous Polymers through Capillaries, *J. Appl. Phys.* 27, 454 (1956)
- [50] M. M. Denn, Issues in viscoelastic fluid mechanics, *Annu. Rev. Fluid Mech.* 22, 13 (1990)
- [51] Volfrango Bertola, Bernard Meulenbroek, Christian Wagner, Cornelis Storm, Alexander Morozov, Wim van Saarloos, Daniel Bonn, Experimental Evidence for an Intrinsic Route to Polymer Melt Fracture Phenomena: A Nonlinear Instability of Viscoelastic Poiseuille Flow, *Phys. Rev. Lett.* 90 (2003) 114502.
- [52] L. T. N. Périnet, D. Juric, Numerical simulation of faraday waves, *J. Fluid Mech.* 635 (2009) 1-26.
- [53] J. Eggers, Universal pinching of 3d axisymmetrical free-surface flow, *Phys. Rev. Lett.* 71 (1993) 3458.
- [54] J. McLean, P. Saffman, The effect of surface tension on the shape of fingers in a hele-shaw cell, *J. Fluid Mech.* 102 (1981) 455-469.
- [55] D. Hong, J. Langer, Analytic theory of the selection mechanism in the Saffman-Taylor problem, *Phys. Rev. Lett.* 56 (1986) 2032-2035.
- [56] B. Shraiman, Velocity selection in the Saffman-Taylor problem, *Phys. Rev. Lett.* 56 (1986) 2028-2031.
- [57] R. Combescot, T. Dombre, V. Hakim, Y. Pomeau, Shape selection of Saffman-Taylor fingers, *Phys. Rev. Lett.* 56 (1986) 2036-2039.
- [58] B. H. Zimm, Dynamics of polymer molecules in dilute solution, *J. Chem. Phys.* 24 (1956) 269.
- [59] A. Lindner, J. Vermant, D. Bonn, How to obtain the elongational viscosity of dilute polymer solutions?, *Physica A: Statistical Mechanics and its Applications* 319 (2003) 125-133.
- [60] C. Clanet and J. C. Lasheras, Transition from dripping to jetting, *J. Fluid Mech.* 383 (1999) 307-326.
- [61] A. Rothert, R. Richter, I. Rehberg, Formation of a drop: viscosity dependence of three flow regimes, *New J. Phys.* 5 (2003).
- [62] H. Chang, E. Demekhin, E. Kalaidin, Iterated stretching of viscoelastic jets, *Phys. Fluids* 11 (1999) 1717-1737.
- [63] M. Stelter, G. Brenn, A.L. Yarin, R.P. Singh, F. Durst, Validation and application of a novel elongational device for polymer solutions, *J. Rheol.*, 44 (2001) 595-616.
- [64] M. Oliveira, G. McKinley, Iterated stretching and multiple beads-on-a-string phenomena in dilute solutions of highly extensible flexible polymers, *Phys. Fluids* 17 (2005) 071704.
- [65] M. S. N. Oliveira, R. Yeh, G. H. McKinley, Iterated stretching, extensional rheology and formation of beads-on-a-string structures in polymer solutions, *J. Non-Newtonian Fluid Mech.* 137 (2006) 137-148.
- [66] R. Sattler, C. Wagner, J. Eggers, Blistering pattern and formation of nanofibers in capillary thinning of polymer solutions, *Phys. Rev. Lett.* 100 (2008) 164502.
- [67] B. Carroll, Equilibrium conformations of liquid-drops on thin cylinders under forces of capillarity - a theory for the roll-up process, *Langmuir* 2 (1986) 248-250.
- [68] D. James, J. Saringer, Extensional flow of dilute polymer-solutions, *J. Fluid Mech.* 97 (1980), 655-76.
- [69] T. Kume, T. Hashimoto, T. Takahashi, G. Fuller, Rheo-optical studies of shear-induced structures in semidilute polystyrene solutions, *Macromolecules* 30 (1997) 7232-7236.
- [70] R. Sattler, A. Kityk, C. Wagner, Molecular configurations in the droplet detachment process of a complex liquid, *Phys. Rev. E* 75 (2007) 051805.
- [71] R. Chuoque, P. v. Meurs, C. v. d. Poel, The instability of slow, immiscible, viscous liquid-liquid displacements in permeable media, *Pet. Trans. AIME* 216 (1959) 188.
- [72] P. Tabeling, A. Libchaber, Film draining and the Saffman-Taylor problem, *Phys. Rev. A* 33 (1986) 794-796.
- [73] S. Nguyen, H. Henry, M. Plapp, privat communication.
- [74] L. Kondic, M. J. Shelley, P. Palfy-Muhoray, Non-Newtonian Hele-Shaw flow and the Saffman-Taylor instability, *Phys. Rev. Lett.* 80 (1998) 1433-1436
- [75] A. Lindner, D. Bonn, J. Meunier, Viscous fingering in a shear-thinning fluid, *Phys. Fluids* 12 (2000) 256-261.
- [76] M. Rabaud, Y. Couder, N. Gerard, Dynamics and stability of anomalous Saffman-Taylor fingers, *Phys. Rev. A* 37 (1988) 935-947.
- [77] E. CorveraPoire, M. BenAmar, Finger behavior of a shear thinning fluid in a hele-shaw cell, *Phys. Rev. Lett.* 81 (1998) 2048-2051.
- [78] L. Matthiesen, *Annal. Phys. u. Che.* 5 (14) 107.
- [79] Rayleigh, Numerical simulation of Faraday waves, *Phil. Mag. a Jour. of Sc.* 5 (1883) 229.
- [80] T. B. Benjamin, F. Ursell, Numerical simulation of faraday waves, *Proc. R. Soc. London, Ser. A* 225 (1954) 505.
- [81] K. Kumar, L. Tuckerman, Parametric-instability of the interface between 2 fluids, *J. Fluid Mech.* 279 (1994), 49-68.
- [82] H. Muller, H. Wittmer, C. Wagner, J. Albers, K. Knorr, Analytic stability theory for Faraday waves and the observation of the harmonic surface response, *Phys. Rev. Lett.* 78 (1997) 2357-2360.
- [83] H. Arbell, J. Fineberg, Spatial and temporal dynamics of two interacting modes in parametrically driven surface waves, *Phys. Rev. Lett.* 81 (1998) 4384-4387.
- [84] W. Edwards, S. Fauve, Patterns and quasi-patterns in the Faraday experiment, *J. Fluid Mech.* 278 (1994) 123-148.
- [85] A. Kityk, J. Embs, V. Mekhonoshin, C. Wagner, Spatiotemporal characterization of interfacial Faraday waves by means of a light absorption technique, *Phys. Rev. E* 72 (2005) 036209.
- [86] P. Chen, J. Vinals, Pattern selection in Faraday waves, *Phys. Rev. Lett.* 79 (1997) 2670-2673.